Sensors and Materials, Vol. 36, No. 9 (2024) 3767–3778
MYU Tokyo

S & M 3765

Optimizing Sensor-grade High-strength Low-alloy Steel: Effects of Cyclic Heat Treatment

Shih-Chen Shi* and Dun-Kai Ko

Department of Mechanical Engineering, National Cheng Kung University (NCKU),
No. 1, University Road, Tainan 70101, Taiwan

(Received April 1, 2024; accepted July 19, 2024)

Keywords: sensor, sustainability process, grain refinement, microstructure

Demand for optimized high-strength, low-alloy steel used in sensor applications and as load elements is rising. Achieving strength through grain refinement while preserving toughness is both practical and sustainable. Severe plastic deformation, which is necessary for this effect, is not always feasible owing to constraints in manufacturing and product forms, such as welding or significant components. In this study, we explored grain refinement via cyclic heat treatment to circumvent these limitations, employing varied heating (medium-frequency heating and salt bath treatment), and cooling (water quenching, oil quenching, and air cooling) rates, and additional heat treatments. The process aimed at refining grains through repeated austenite to martensite transformations. The analysis covered microstructural impacts on mechanical properties and grain refinement efficiency. Comparatively, cyclic heat treatment enhanced tensile strength by 180 MPa and reduced grain size to 5.72 μm, outperforming quenching and tempering methods. Additionally, the efficacy of grain refinement improved with more cyclic heat treatment cycles.

1. Introduction

In response to the Sustainable Development Goals, the need for carbon reduction and environmental conservation drives the critical development of efficient materials and processes.[1–5] High-strength low-alloy (HSLA) steel is vital for heavy industries, especially automotive, owing to its cost-effectiveness and simple production. Recently, HSLA for sensor applications has been significantly optimized.[6,7] Evolving demands for material strength and toughness necessitate enhancements in mechanical properties. Strengthening methods include solid solution strengthening, precipitation hardening, dispersion hardening, strain hardening, grain refinement, and phase transformation hardening. Most methods compromise toughness for increased strength. Grain refinement simultaneously elevates toughness and strength, decreasing grain size to augment grain boundary areas. These boundaries, rich in surface energy and dislocation impediments, effectively bolster material strength without significantly impairing toughness. Severe plastic deformation, a predominant grain refinement technique, has been extensively studied for effectiveness.[8–16] More rigid materials necessitated grain refinement

*Corresponding author: e-mail: scshi@mail.ncku.edu.tw
https://doi.org/10.18494/SAM5058

ISSN 0914-4935
https://myukk.org/

through large-scale machinery and energy-intensive annealing or thermo-mechanical processes, complicating the procedure.[17,18] Owing to process and material constraints, cyclic heat treatment offers an alternative for grain refinement. This method leverages repeated phase transitions between austenite and martensite. Rapidly heating steel above the Ae_3 temperature and immediately quenching after full austenitization prevent grain growth from excessive austenitization, thus reducing grain size. Numerous studies support the efficacy of cyclic heat treatment for grain refinement. For example, Shibata *et al.*[19] achieved an average austenite grain size of 4.5 μm only by cyclic heat treatment on 0.46C–0.84Mn (mass%) without plastic deformation. Furuhara *et al.*[20] conducted cyclic heat treatment and air cooling (AC) on 0.35C–1.05Cr–0.17Mo (mass%) to obtain fine-grained ferrite with an average grain size of 2.2 μm. In addition, many studies have reported on the critical factors of grain refinement,[21] which precisely control the following vital factors: heating rate,[22] quenching rate,[23–25] the temperature setting of austenitization,[22,26] constant-temperature duration, and several cyclic heat treatments, as well as a secondary phase to control grain growth.[27,28]

While repeated heat treatments have proven effective for medium-carbon steels, their application to low-carbon steels is less studied. Low-carbon steels exhibit low hardenability, are favored for their superior weldability, and are indispensable in welding applications. This characteristic impedes their complete martensitic transformation, restricting the number of nucleation sites and, thus, the grain refinement potential. The relatively high Ae_3 temperature facilitates austenite grain growth during repeated phase changes, further diminishing grain refinement efficacy.

In this study, we employed HSLA steel to evaluate the effects of various heating methods, including high-frequency heating and salt bath (SB) treatment, and cooling rates from water and oil quenching (OQ) to AC. We aimed to elucidate the correlation between microstructure, mechanical properties, grain refinement degree, and strength enhancement. The goal was to optimize grain refinement, enhancing the applicability of low-carbon steels in the sensor application field.

2. Materials and Methods

2.1 Materials and process

In this study, we focused on HSLA steel with 0.25% carbon and 0.7% each of Cr and Ni. It was noted for its superior mechanical properties and usage in high-strength structural applications, particularly for load bearing. The emphasis was on enhancing product strength and toughness. The A_{e3} temperature, essential for austenitizing heat treatment, was determined to be 798 °C. The cyclic heat treatment process involved heating the steel to 900 °C to achieve uniform austenitization, as depicted in Fig. 1. This process was followed by water quenching (WQ) and repeated treatments to refine the grain structure. In Table 1, route A employed medium-frequency (MF) heating to 820 °C, cooling, and repeating thrice for finer grains. The final cooling method dictated the microstructure; WQ resulted in martensite, while AC produced ferrite and pearlite, with martensite samples tempered at 550 °C. Route B utilized SB treatment

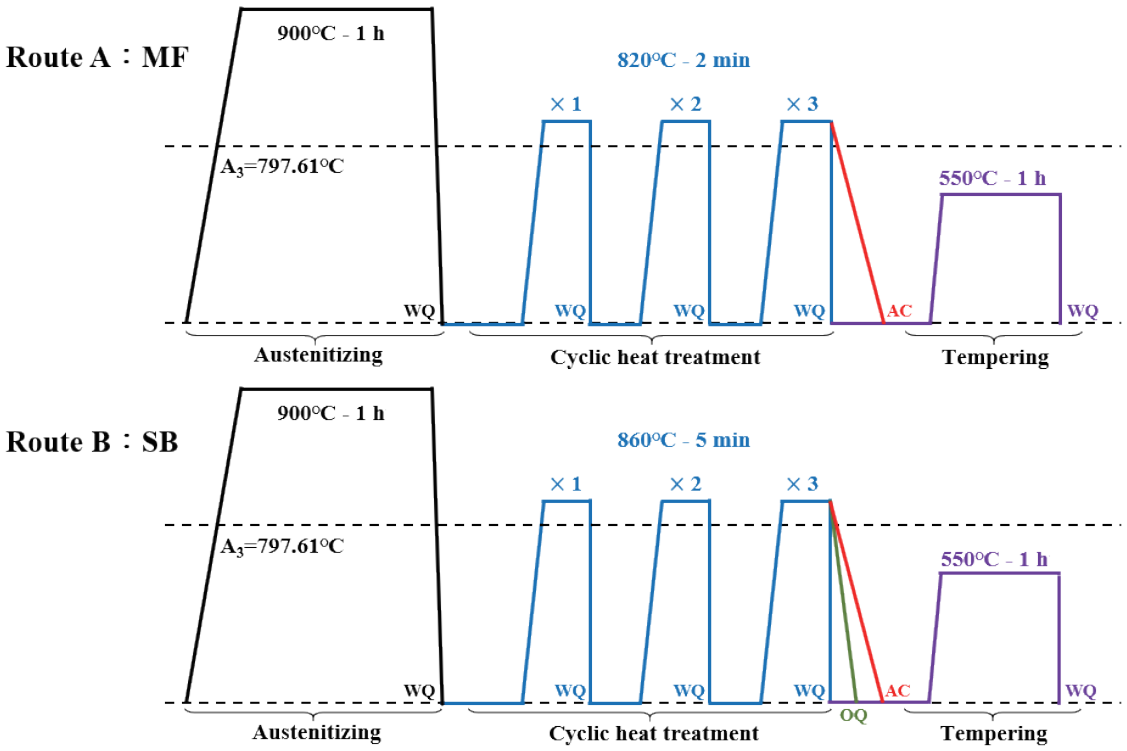

Fig. 1. (Color online) Schematic diagram of the grain refinement treatment process.

Table 1
Cyclic heat treatment process with MF heating.

MF: increase temperature to 820 °C and then cool down	
MFAC1	820 °C AC
MFAC2	820 °C WQ + 820 °C AC
MFAC3	820 °C WQ + 820 °C WQ + 820 °C AC
MFWQ1	820 °C WQ
MFWQ2	820 °C WQ + 820 °C WQ
MFWQ3	820 °C WQ + 820 °C WQ + 820 °C WQ

Number: total number of heat treatments, where the final heat treatment is cooling to obtain desired microstructure and WQ is used to improve grain refinement efficiency

to heat the steel to 860 °C for 5 min, as shown in Table 2. We compared the effects of treatment repetitions and cooling rates on strength, controlled microstructure via cooling, and enhanced martensite toughness through tempering. The process of quenching and tempering (QT) involved heating the steel to 900 °C, followed by WQ, and then tempering it at 550 °C to achieve tempered martensite. After each treatment, samples were reserved for tensile testing, metallographic analysis, hardness measurement, and grain size evaluation.

Table 2
Cyclic heat treatment with salt-bath heating.

SB: immerse in an 860 ℃ SB furnace for 5 min and then cool down	
SBAC1	860 ℃ AC
SBAC2	860 ℃ WQ + 860 ℃ AC
SBOQ1	860 ℃ OQ
SBOQ2	860 ℃ WQ + 860 ℃ OQ
SBOQ3	860 ℃ WQ + 860 ℃ WQ + 860 ℃ OQ
SBWQ1	860 ℃ WQ
SBWQ2	860 ℃ WQ + 860 ℃ WQ
SBWQ3	860 ℃ WQ + 860 ℃ WQ + 860 ℃ WQ

2.2 Tensile tests

To compare the mechanical properties of different microstructures, a universal tensile testing machine (SHIMADZU AG-X plus) was used to conduct uniaxial tensile testing at 25 ℃. The size of the test bar was the same as that of ASTM E8 sample 2, with a strain rate set at 8.3×10^{-4} s^{-1}. Subsequently, 10 mm of the sample was cut from the test bar for microstructural observation.

2.3 Microstructural observation

Before microstructural analysis, samples underwent mechanical grinding (from #320 to #4000), polishing with 1 μm alumina powder, and etching in 3% Nital solution for 1 min. Subsequent cleaning involved an ultrasonic cleaner, alcohol wash, and drying. We employed a laser scanning microscope (VK 9700, Keyence) to observe the microstructures of tempered martensite, ferrite, and pearlite. For grain boundary etching, a saturated aqueous picric acid solution (5 g of picric acid in 100 ml of distilled water) was used. Samples were etched at 90 ℃ for 3 min, then ultrasonically cleaned, alcohol-washed, dried, and examined with the same microscope. Average grain size was determined via the ASTM E112 linear intercept method, facilitating the quantitative analysis of grain refinement effects.

3. Results and Discussion

Cooling rate significantly affected the microstructure, as demonstrated by samples undergoing QT, AC, OQ, and WQ, as detailed in Fig. 2. Fast cooling (WQ and OQ) resulted in uniformly tempered martensite. In contrast, AC yielded a mix of initially precipitated ferrite and refined pearlite due to its slower rate, hindering the formation of a high-strength structure. However, ferrite and pearlite exhibited good ductility. Thus, cooling conditions should align with product requirements. As the different cooling rates determined the microstructure, samples treated with QT, AC, OQ, and WQ were as shown in Fig. 3. In particular, it was observed that owing to the fast-cooling rates of quenching (i.e., WQ and OQ), the microstructure was uniformly tempered martensite.

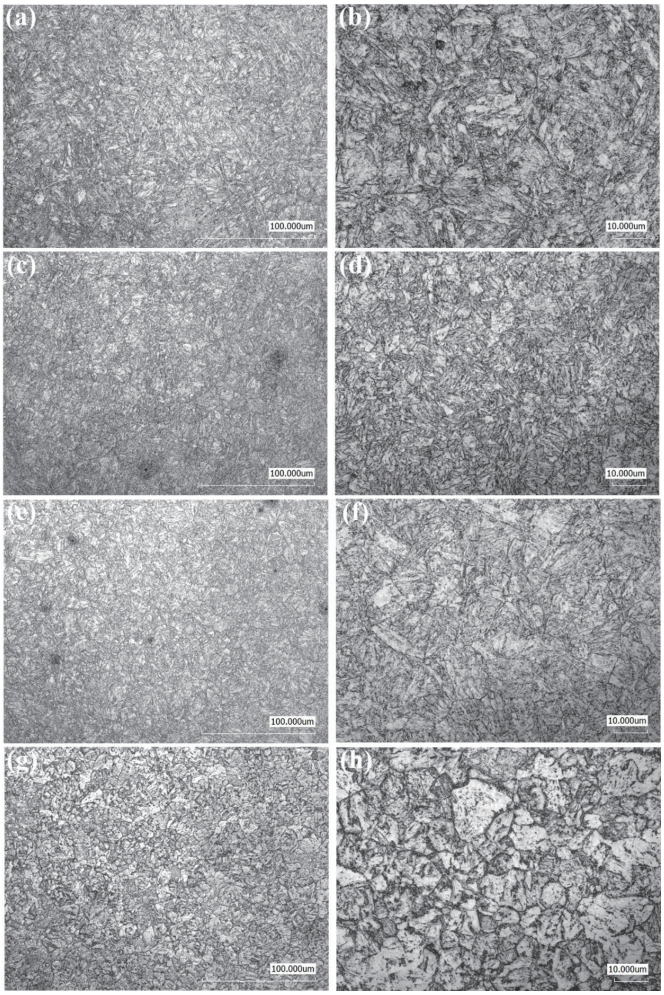

Fig. 2. Metallographic microstructures: (a), (c), (e), and (g) 500×; (b), (d), (f), and (h) 1500×. (a) and (b) QT; (c) and (d) WQ; (e) and (f) OQ; (g) and (h) AC.

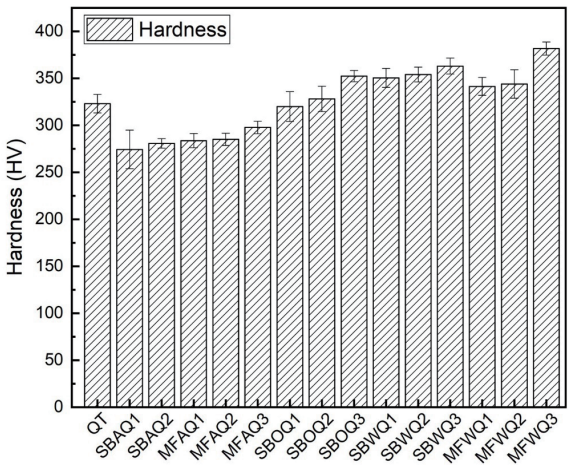

Fig. 3. Hardness distribution of different heat treatments.

In contrast, the air-cooled sample showed a microstructure of initially precipitated ferrite and refined pearlite. A high-strength structure could not be formed because the cooling rate was slower than the above quenching methods. Nevertheless, ferrite and pearlite had relatively good ductility. The cooling conditions could be set according to the requirements of the target products. Cooling rates significantly affect microstructure, as demonstrated by samples undergoing QT, AC, OQ, and WQ. Fast cooling (WQ and OQ) results in uniformly tempered martensite.

In contrast, AC yields a mix of initially precipitated ferrite and refined pearlite owing to its lower rate, hindering the formation of a high-strength structure. However, ferrite and pearlite exhibit good ductility. Thus, cooling conditions should align with product requirements.

Figure 3 shows that MF heating yielded higher heating rates and hardness under identical cooling conditions than SB heating. Specifically, MF heating enhanced grain refinement, correlating with increased hardness. The sample subjected to MF heating and the triple WQ (MFWQ3) exhibited the highest hardness at 381 HV. Conversely, the SB-heated and once-air-cooled sample (SBAC1) showed the lowest hardness at 274 HV. For context, a QT sample displayed a hardness of 323 HV.

The average grain diameters obtained under various heat treatments were assessed on the ground and polished samples etched with saturated picric acid at high temperatures, with findings depicted in Figs. 4 and 5. QT samples were imaged at 500× magnification, whereas

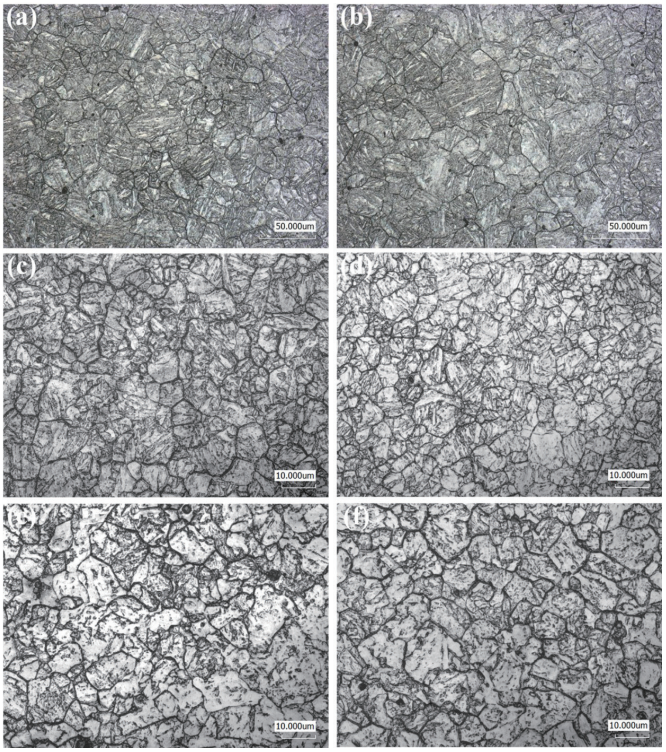

Fig. 4. Etched grains with QT and MF heating: (a) and (b) 500×; (c), (d), (e), and (f) 1500×. (a) and (b) QT; (c) MFWQ1; (d) MFWQ3; (e) MFAC1; (f) MFAC3.

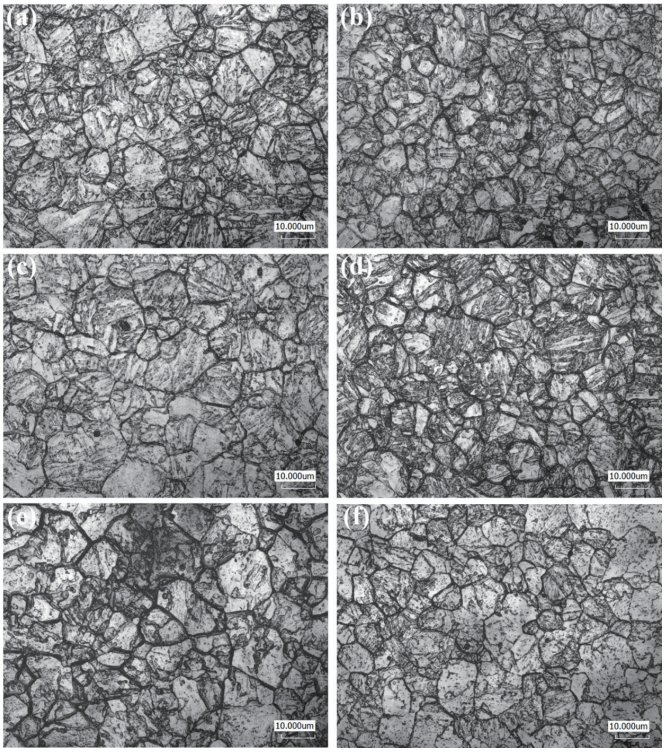

Fig. 5. Etched grains with SB heating: (a), (b), (c), (d), (e), and (f) 1500×. (a) SBWQ1; (b) SBWQ3; (c) SBOQ1; (d) SBOQ3; (e) SBAC1; (f) SBAC3.

other grain-refined samples were captured at 1500×, illustrating significant grain refinement. MFWQ3 achieved a minimum average grain diameter of 5.72 μm and a grain size of 11.5. Average grain diameter increased with fewer heat treatments and lower cooling rates, as evidenced by SBAC1 exhibiting the largest grains, with a size of 10 and an average diameter of 9.44 μm. QT samples showed a grain size of 8.5 and an average diameter of 21.08 μm. These results confirmed that the experimental heat treatments effectively refined grain sizes beyond those of QT samples, simultaneously enhancing hardness.

Tensile test outcomes at room temperature for grain-refined samples (Figs. 6 and 7) revealed enhanced tensile strength with grain size reduction. WQ samples exhibited superior tensile strength compared with their QT counterparts, with MFWQ3 displaying the highest value at 1102 MPa. Conversely, QT samples demonstrated a tensile strength of 913 MPa, indicating a deficit of 180 MPa relative to MFWQ3. Tensile strength diminished across WQ, OQ, and AC samples, with SBAC1 recording the lowest at 868 MPa. Despite smaller grains, grain-refined samples maintained superior ductility (~30% fracture strain) over original QT samples, enhancing strength while preserving toughness. MFAQ3 matched the tensile strength of QT treatments, suggesting that AC-induced ferrite and pearlite offered improved ductility versus tempered martensite. Grain refinement thus broadened potential steel applications by optimizing strength and ductility. Figures 6 and 7 show a constant flow stress following a drop in yield strength, indicative of Lüders deformation. This deformation was more pronounced in WQ and

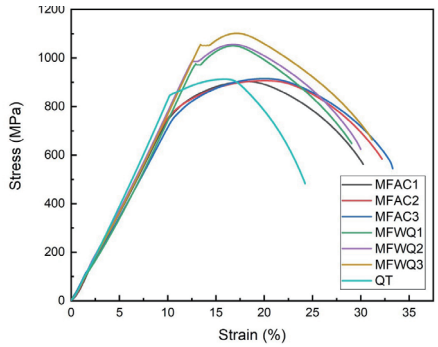

Fig. 6. (Color online) Tensile test results of samples with grain refinement and MF heating.

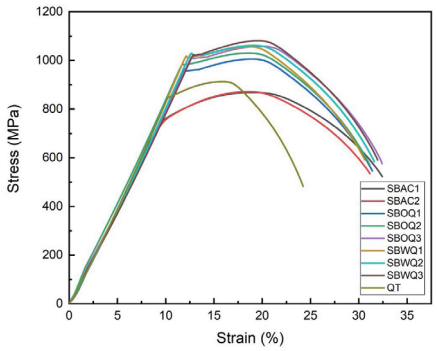

Fig. 7. (Color online) Tensile test results of samples with grain refinement and SB treatment.

OQ samples than in AC samples as grain size diminished, with a notable increase in Lüders strain. For instance, SB-treated samples exhibited a Lüders strain of 2.1% at a grain size of 6.33 μm, compared with 0.3% at 18.74 μm. The phenomenon aligned with Cottrell's theory, suggesting that dislocation movement, constrained by the Cottrell atmosphere, required overcoming a higher external force for yielding. Subsequent deformation occurred at lower stress levels after dislocations escaped the Cottrell atmosphere. Grain refinement escalated strain hardening within the Lüders band, necessitating higher stress for further plastic deformation and explaining the increased Lüders strain in finer-grained samples.

A 10 mm segment from the tensile test bar's fracture section was analyzed via SEM to assess workpiece toughness. Figure 8 shows tempered characteristics across all samples, with dimples indicating ductile fracture modes, characteristic of cup-cone failures. AC samples, composed of ferrite and pearlite, displayed larger dimples than and superior ductility to OQ and WQ samples, which consisted of tempered martensite with similar-sized dimples, suggesting a gradation in ductility from AC, OQ, and WQ samples. SEM images (Fig. 9) contrasted the microstructures of SBAQ3 samples and those subjected to austenitization at 900 °C followed by furnace cooling, revealing fragmented versus typical lamellar pearlite, respectively. This distinction was attributed to refined austenite grains leading to shorter distances between austenite grain boundaries and adjacent pearlite, facilitating faster diffusion. Fine-grained austenite promoted uniform carbon diffusion fields around pearlite, eliminating the need for the concurrent growth of ferrite and cementite and resulting in fragmented pearlite, supporting the efficacy of grain refinement through cyclic heat treatment in enhancing microstructural features. Figures 6 and 7 show that, after the decrease in yield strength, the flow stress was kept almost constant, indicating Lüders deformation in the region. Moreover, as the grain size decreased, the reduction in the yield strength of WQ and OQ samples was more significant than that of AC samples, and the length of the flat region (Lüders strain) also increased considerably. Taking the SB-treated samples as an example, the Lüders strain was 2.1%, where the grain size was 6.33 μm, and only 0.3%, where the grain size was 18.74 μm. In general, Lüders deformation could be understood according to the Cottrell atmosphere.

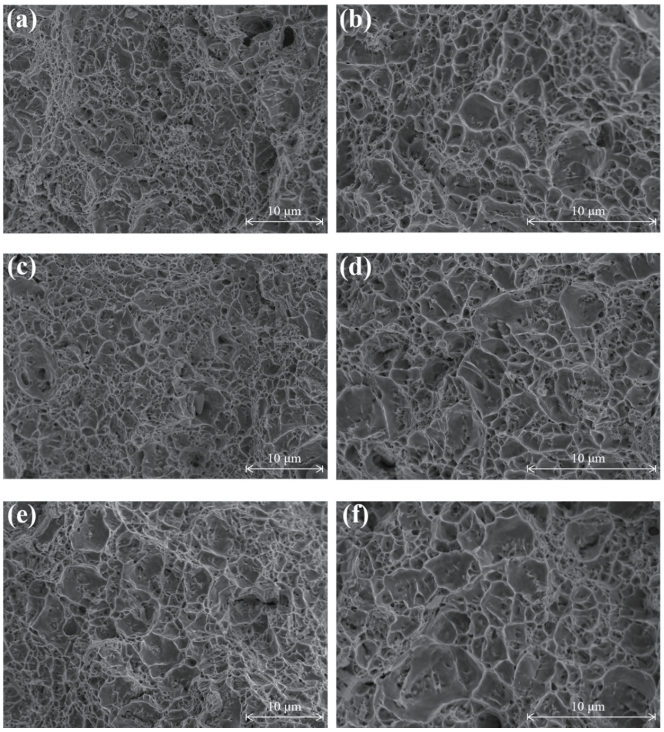

Fig. 8. Fractured section: (a), (c), and (e) 3000×; (b), (d), and (f) 5000×. (a) and (b) WQ; (c) and (d) OQ; (e) and (f) AC.

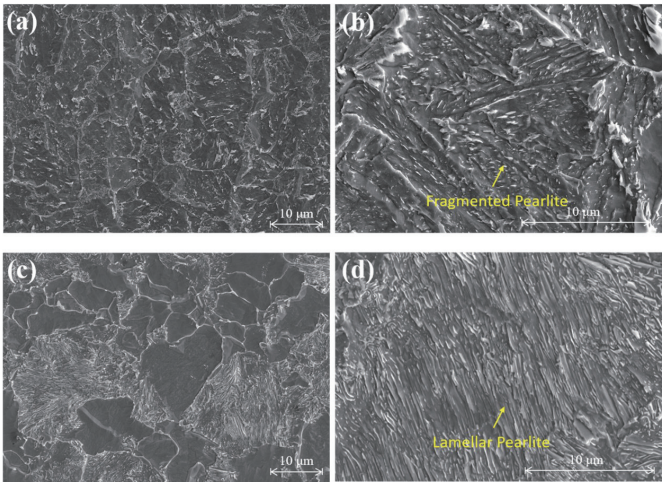

Fig. 9. (Color online) SEM microstructures: (a) and (b) SBAQ3; (c) and (d) 900 ℃ + FC.

Figure 9 shows the SEM results of the sample microstructures. Figures 9(a) and 9(b) show the microstructures of SBAQ3 samples, whereas Figs. 9(c) and 9(d) show the results after austenitization at 900 ℃ and furnace cooling (900 ℃ + FC). Figures 9(a) and 9(b) show

fragmented pearlite, whereas Figs. 9(c) and 9(d) show typical lamellar pearlite. Shibata *et al.* also observed fragmented pearlite in medium-carbon steels and explained that refined austenite grains were transformed into fragmented pearlite.[19] When the grain size of austenite was relatively small, the distance between the austenite grain boundary (or the triple junction of the austenite grain boundary) and the adjacent pearlite became shorter. The high-density, fine-grained austenite grain boundaries served as a fast channel for diffusion. When fine-grained austenite (e.g., dγ 11.1 μm) existed, the carbon diffusion fields around the adjacent pearlite could overlap to become more uniform. As such, ferrite and cementite no longer need to grow in accordance with each other, nor do they maintain the typical lamellar morphology. This was considered the possible reason for the formation of fragmented pearlite in the transformed microstructure of fine-grained austenite in low-carbon steels, proving that grain refinement was effectively achieved by cyclic heat treatment.

During plastic deformation, the dislocations had to break down the restriction of the Cottrell atmosphere to move. Therefore, yielding could only be caused when external force increased (upper yield point appeared). After the dislocations had broken free from the Cottrell atmosphere, they could move under relatively low stress (a lower yield point appeared), causing further deformation at lower stress (lower yield point). The propagation of the Lüders band required the strain hardening of the locally yielded region to reach the undeformed regions, requiring higher stress to initiate plastic deformation. Owing to grain refinement, the strain hardening required within the Lüders band increased as the grain size decreased. This may be why grain-refined samples had an enormous Lüders strain compared with coarser samples, which verified the grain refinement effect.

Figure 10 shows the Hall–Petch relationship, plotting tensile strength against the inverse square root of average grain diameter for samples subjected to various heat treatments. This plot

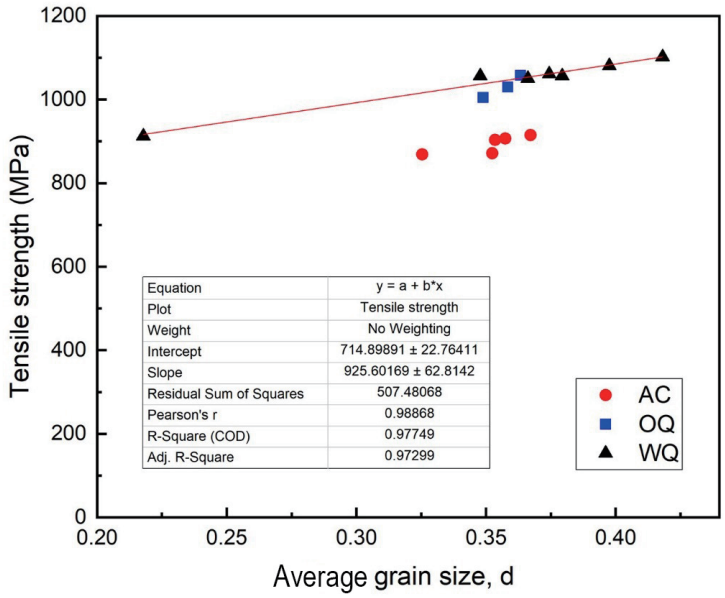

Fig. 10. (Color online) Grain refinement Hall–Petch relationship.

confirmed a linear correlation between tensile strength and the −1/2 power of average grain diameter, substantiating the Hall–Petch relationship. However, owing to distinct microstructures, AC samples exhibited a deviation in tensile strength. The data distribution further demonstrated that cyclic heat treatment yielded smaller grain sizes than QT samples, indicating that grain refinement had effectively enhanced strength. Hence, the observation of the grain structure provides a viable method for evaluating the strength of HSLA steels.

4. Conclusions

In this study, we demonstrated that cyclic heat treatment effectively refined grains without inducing plastic deformation, enhancing material strength and toughness. Specifically, high heating and cooling rates, particularly with MF heating and thrice WQ, reduced the grain size to 5.72 μm. This refinement increased the tensile strength to 1102 MPa and maintained elongation at 30%, marking a 180 MPa improvement over traditional QT methods. Analyses of the Lüders strain, SEM microstructures, and the Hall–Petch relationship confirmed significant grain refinement. Moreover, grain refinement enhanced the strength of pearlite and ferrite to match that of QT samples while improving elongation, broadening material applications, and addressing mechanical property limitations. Nonetheless, the extended duration of cyclic heat treatment compared with traditional methods suggested the need for further research to balance strength enhancement with production efficiency and cost. This ecofriendly and efficient strengthening method allows us to attain sensor application-grade processes.

Funding

This work was financially supported by the National Science and Technology Council, Taiwan (grant numbers 111-2221-E-006-145, 111-2221-E-006-147-MY2, 111-2221-E-006-133, and 112-2221-E-006 -173).

Acknowledgments

The authors gratefully acknowledge the use of the EM000700 equipment belonging to the Core Facility Center of National Cheng Kung University. The authors gratefully acknowledge the Core Facility Center of National Cheng Kung University. This research was partly supported by the Higher Education Sprout Project, Ministry of Education, Headquarters of University Advancement at National Cheng Kung University (NCKU).

Author contributions

Conceptualization: Shih-Chen Shi; Methodology: Shih-Chen Shi, Dun-Kai Ko; Formal analysis and investigation: Shih-Chen Shi, Dun-Kai Ko; Writing—original draft preparation: Dun-Kai Ko; Writing—review and editing: Shih-Chen Shi; Funding acquisition: Shih-Chen Shi; Resources: Shih-Chen Shi, Dun-Kai Ko; Supervision: Shih-Chen Shi.

Competing Interests

The authors have no relevant financial or non-financial interests to disclose.

References

1 S.-C. Shi, C.-F. Chen, G.-M. Hsu, J.-S. Hwang, S. Chattopadhyay, Z.-H. Lan, K.-H. Chen, and L.-C. Chen: Appl. Phys. Lett. **87** (2005) 203103.
2 S.-C. Shi and J.-Y. Wu: Surf. Coat. Technol. **350** (2018) 1045. https://doi.org/10.1016/j.surfcoat.2018.02.067
3 D. Rahmadiawan and S.-C. Shi: Sci. Rep. **14** (2024) 9217. https://doi.org/10.1038/s41598-024-59010-w
4 D. Rahmadiawan, H. Abral, S.-C. Shi, T.-T. Huang, R. Zainul, A. Ambiyar, and H. Nurdin: Tribol. Ind. **45** (2023) 367. https://doi.org/10.24874/ti.1482.05.23.06
5 D. Rahmadiawan, S.-C. Shi, Z. Fuadi, H. Abral, N. Putra, R. Irwansyah, D. Gasni, and A. M. Fathoni: J. Tribologi **39** (2023) 36.
6 T. Kosec, V. Kuhar, A. Kranjc, V. Malnarič, B. Belingar, and A. Legat: Sensors **19** (2019) 1956. https://doi.org/10.3390/s19081956
7 S.-C. Shi, W.-C. Wang, and D.-K. Ko: Metals **12** (2022) 242. https://doi.org/10.3390/met12020242
8 V. V. Stolyarov, Y. T. Zhu, T. C. Lowe, and R. Z. Valiev: Mater. Sci. Eng., A **303** (2001) 82. https://doi.org/10.1016/S0921-5093(00)01884-0
9 N. Tsuji, R. Ueji, and Y. Minamino: Scr. Mater. **47** (2002) 69. https://doi.org/10.1016/S1359-6462(02)00088-X
10 Y. I. Son, Y. K. Lee, K.-T. Park, C. S. Lee, and D. H. Shin: Acta Mater. **53** (2005) 3125. https://doi.org/10.1016/j.actamat.2005.02.015
11 A. Azushima, R. Kopp, A. Korhonen, D. Y. Yang, F. Micari, G. D. Lahoti, P. Groche, J. Yanagimoto, N. Tsuji, and A. Rosochowski: CIRP Annals **57** (2008) 716. https://doi.org/10.1016/j.cirp.2008.09.005
12 M. Okayasu, K. Sato, M. Mizuno, D. Y. Hwang, and D. H. Shin: Int. J. Fatigue **30** (2008) 1358. https://doi.org/10.1016/j.ijfatigue.2007.10.011
13 N. Tsuji, N. Kamikawa, R. Ueji, N. Takata, H. Koyama, and D. Terada: ISIJ Int. **48** (2008) 1114. https://doi.org/10.2355/isijinternational.48.1114
14 M. Calcagnotto, D. Ponge, and D. Raabe: Mater. Sci. Eng., A **527** (2010) 7832. https://doi.org/10.1016/j.msea.2010.08.062
15 I. F. Mohamed, Y. Yonenaga, S. Lee, K. Edalati, and Z. Horita: Mater. Sci. Eng., A **627** (2015) 111. https://doi.org/10.1016/j.msea.2014.12.117
16 S. Amani, G. Faraji, and K. Abrinia: J. Manuf. Processes **28** (2017) 197. https://doi.org/10.1016/j.jmapro.2017.06.007
17 Y. Okitsu, N. Takata, and N. Tsuji: Scr. Mater. **60** (2009) 76. https://doi.org/10.1016/j.scriptamat.2008.09.002
18 N. Tsuji, R. Gholizadeh, R. Ueji, N. Kamikawa, L. Zhao, Y. Tian, Y. Bai, and A. Shibata: Mater. Trans. **60** (2019) 1518. https://doi.org/10.2320/matertrans.MF201936
19 A. Shibata, S. Daido, D. Terada, and N. Tsuji: Mater. Trans. **54** (2013) 1570. https://doi.org/10.2320/matertrans.MH201312
20 T. Furuhara, K. Kikumoto, H. Saito, T. Sekine, T. Ogawa, S. Morito, and T. Maki: ISIJ Int. **48** (2008) 1038. https://doi.org/10.2355/isijinternational.48.1038
21 T. Furuhara, N. Takayama, and G. Miyamoto: Mater. Sci. Forum **638** (2010) 3044. https://doi.org/10.4028/www.scientific.net/MSF.638-642.3044
22 R. A. M. Napitupulu: IOP Conf. Ser.: Mater. Sci. Eng. **237** (2017) 012038. https://doi.org/10.1088/1757-899X/237/1/012038
23 H. Zhao and E. J. Palmiere: Mater. Charact. **158** (2019) 109990. https://doi.org/10.1016/j.matchar.2019.109990
24 M. Olasolo, P. Uranga, J. M. Rodriguez-Ibabe, and B. López: Mater. Sci. Eng., A **528** (2011) 2559. https://doi.org/10.1016/j.msea.2010.11.078
25 H. Zhao and E. J. Palmiere: Metall. Mater. Trans. A **48** (2017) 3389. https://doi.org/10.1007/s11661-017-3987-z
26 S. Maropoulos, S. Karagiannis, and N. Ridley: Mater. Sci. Eng., A **483** (2008) 735. https://doi.org/10.1016/j.msea.2006.11.172
27 H.-J. Kestenbach, J. A. Rodrigues, and J. R. Dermonde: Mater. Sci. Technol. **5** (1989) 29. https://doi.org/10.1179/mst.1989.5.1.29
28 J. R. Wilcox and R. W. K. Honeycombe: Mater. Sci. Technol. **3** (1987) 849. https://doi.org/10.1179/mst.1987.3.10.849